IMPROVED EXACT STRIP POSTBUCKLING ANALYSIS FOR ANISOTROPIC PLATES WITH FIXED, FREE AND STRAIGHT EDGES

Bin Che, David Kennedy, Carol Featherston
Cardiff School of Engineering, Cardiff University, Queen's Buildings, The Parade,
Cardiff CF24 3AA, United Kingdom
cheb@cf.ac.uk; kennedyd@cf.ac.uk; featherstonca@cf.ac.uk

Keywords: *plates, postbuckling, composite, exact strip, Wittrick-Williams algorithm*

Abstract

The paper presents recent developments in exact strip postbuckling analysis for anisotropic plates with combined in-plane loading and various in-plane edge conditions. The analysis improves the accuracy of the postbuckling mode and the consequent prediction of stresses and strains in the postbuckling range. Plates are divided into longitudinal strips, for which the governing equilibrium equations are derived and solved analytically. Implementation of the improved analysis into the exact strip software VICONOPT enables accurate stress distributions to be found for each stage of the postbuckling analysis. Numerical results are presented and compared with previous results from VICONOPT and finite element analysis for validation.

Principal Nomenclature

$\mathbf{A}_i,\mathbf{B}_i,\mathbf{D}_i$	membrane, bending-membrane and flexural stiffness matrices for node i
a	length of plate
$b_i,$	width of strip i
$\mathbf{D}$	displacement vector
f	eigenparameter, i.e. load factor
f^*	trial value of f
$\mathbf{I}_5$	unit matrix of order 5
J	number of eigenvalues below f^*
J_0	number of fixed end eigenvalues below f^*
J_m	number of fixed end eigenvalues of member m below f^*
$\mathbf{k}_m$	member stiffness matrix
$\mathbf{K}(f)$	global stiffness matrix
n	number of strips
N_{xij},N_{yij},N_{xyij}	stress resultants at node i
$\mathbf{O}_5$	null matrix of order 5
$\mathbf{P}$	perturbation force vector
$s\{\mathbf{K}(f)\}$	sign count of $\mathbf{K}(f)$
u_{ij},v_{ij}	in-plane displacements at node i
V_{xi}, V_{yi}, V_{xyi}	work done by applied loads
w_{ij},ψ_{ij}	out-of-plane displacements and rotations at node i
x, y, z	longitudinal, transverse and lateral directions
$\varepsilon_{xij},\varepsilon_{yij},\gamma_{xyij}$	membrane strains at node i
$\eta_{xij}, \eta_{yij}, \eta_{xyij}$	parameters used in effective stress resultant calculations
$\kappa_{xij},\kappa_{yij},\kappa_{xyij}$	curvatures at node i
λ	longitudinal half-wavelength
ω_i	coefficient, $= \pi b_i/\lambda$

Subscripts

i	node reference number
j	solution case: $j = 0, c, s, C, S$ give terms to be multiplied by factors 1, $\cos \pi x/\lambda$, $\sin \pi x/\lambda$, $\cos 2\pi x/\lambda$, $\sin 2\pi x/\lambda$
m	member
x, y, xy	longitudinal, transverse, shear

1 Introduction

Minimising the weight of aircraft structures is a major objective in reducing the manufacturing cost, fuel consumption and environmental

impact. To achieve this objective, composite materials are commonly used to replace traditional metals, to ensure low mass and high performance. Additionally, the postbuckling reserve of strength is often considered in modern aircraft design, e.g. to reduce the weight of stiffened wing and fuselage panels.

Exact strip analysis provides a reliable efficient approach to aircraft design, which reduces the computation and modelling time when compared with finite element (FE) analysis by avoiding discretisation. This approach gives rapid solutions with satisfactory accuracy, and is therefore of particular benefit in the preliminary design stage. For buckling and vibration problems, the exact strip method leads to a transcendental eigenproblem rather than the linear eigenproblem encountered in FE analysis. Using the Wittrick-Williams algorithm [1], the eigenvalues (i.e. critical buckling load factors or natural frequencies of free vibration) and the corresponding mode shapes of rectangular plates and prismatic stiffened panels can be found efficiently and reliably for any longitudinally invariant loading combination.

The paper outlines recent developments in exact strip postbuckling analysis. The governing in-plane equilibrium equations are derived and solved analytically, using a formulation which extends that of Stein [2] to include fully anisotropic laminates, including the effects of bending-membrane coupling. The accuracy of the postbuckling mode shape and the consequent prediction of stress and strain are thus enhanced in the postbuckling range. Implementation in the exact strip analysis and optimum design software VICONOPT [3] allows the improved mode shapes and stress and strain distributions to be found at each stage of the postbuckling analysis. Numerical results are given and compared with previous VICONOPT results, and also with FE results to validate the proposed analysis.

2   Exact Strip Analysis and Wittrick-Williams Algorithm

The exact strip method provides a reliable alternative approach to FE for accurate solutions and fast analysis of rectangular plates and prismatic plate assemblies. It assumes a continuous distribution of stiffness and mass over the entire structure, so avoiding the discretisation of stiffness and mass to nodal points used in FE analysis. The analysis is based on analytical [4] or numerical [5] solutions to determine the in-plane and out-of-plane deformations of the component plates. The component member stiffness matrices $\mathbf{k}_m$, which include transcendental terms, are assembled into the global stiffness matrix $\mathbf{K}$ for the overall structure. $\mathbf{K}$ relates a finite set of displacements $\mathbf{D}$ and the corresponding perturbation forces $\mathbf{P}$ at the nodes of the structure by

$$\mathbf{KD} = \mathbf{P} \tag{1}$$

The critical buckling loads or natural frequencies of the structure are obtained by finding the eigenvalues from the solution of

$$\mathbf{K}(f)\mathbf{D} = \mathbf{0} \tag{2}$$

where the eigenparameter f is the load factor or frequency. Since $\mathbf{K}(f)$ is a transcendental function of f, Eq. (2) represents a highly nonlinear transcendental eigenproblem which cannot be solved by the standard methods for linear eigenproblems.

The Wittrick-Williams algorithm [1] is a reliable numerical technique for finding the eigenvalues for such a transcendental eigenproblem. Instead of finding the eigenvalues directly, the algorithm counts the number of eigenvalues which lie below any trial value f^* of f, and then converges on them to the required accuracy by bisection or interpolation on the determinant of $\mathbf{K}(f)$ [6]. In its general form, the Wittrick-Williams algorithm can be written as

$$J = J_0 + s\{\mathbf{K}(f^*)\} \tag{3}$$

where J is the number of eigenvalues lying between zero and the trial value f^*; J_0 is the number of eigenvalues which would still be exceeded by f^* if constraints were imposed so as to make all the displacements $\mathbf{D}$ zero; $s\{\mathbf{K}(f^*)\}$ is known as the sign count, i.e. the number of negative diagonal elements of the upper triangular matrix $\mathbf{K}^\Delta(f^*)$ obtained from

$\mathbf{K}(f^*)$ by Gauss elimination [1]. J_0 can be calculated from

$$J_0 = \sum_m J_m \tag{4}$$

where J_m is the number of eigenvalues of member m exceeded at the trial value f^* when its ends are fully restrained.

3 Exact Strip Software VICONOPT

The exact strip software VICONOPT [3] was developed at Cardiff University and has been utilized in research and industry for many years. It covers both isotropic and fully anisotropic prismatic plate assemblies and includes analysis for elastic buckling, local postbuckling and free vibration, as well as an optimum design capability. Typical panel sections that can be analysed by VICONOPT and a typical plate component with in-plate loading are shown in Fig. 1. VICONOPT is coded in Fortran 77 and incorporates the earlier programs VIPASA (Vibration and Instability of Plate Assemblies including Shear and Anisotropy) [4] and VICON (VIPASA with CONstraints) [7].

In the VIPASA analysis, the mode shape of buckling or vibration is assumed to vary sinusoidally in the longitudinal (x) direction. The computation is repeated for a set of user specified half-wavelengths λ and converges to the required eigenvalues for each λ to any required accuracy. Exact solutions are obtained for isotropic and orthotropic panels with simply supported ends and which carry no shear load. In the VICON analysis, Lagrangian multipliers are introduced to couple the responses of different half-wavelengths λ in order to analyse

panels which are anisotropic or carry shear load.

The VIPASA analysis of VICONOPT was first extended to include local postbuckling analysis by Powell *et al.* [8]. Further developments, described fully in [9], have been applied to the multi-level optimisation of an aircraft wing, allowing for postbuckling effects [10]. The postbuckling analysis comprises a number of cycles, each defined by an increment of the longitudinal strain. At each cycle, iterations are performed to converge on consistent values of the postbuckling mode and its amplitude, the total applied load and the distribution of stress across the structure. Instead of using the Wittrick-Williams algorithm for eigenanalysis, Newton iterations are performed to obtain accurate convergence on the postbuckling mode shape, from which the stress distributions are calculated. At each iteration it is necessary to calculate $\mathbf{K}$ and its derivatives with respect to the components of $\mathbf{D}$ [9].

VICONOPT gives a good initial evaluation of load versus end shortening when compared with experimental and FE results. However the predicted postbuckling stress and strain distributions show poor agreement. This is due to the assumptions made in VICONOPT concerning the longitudinal invariance of stress and the sinusoidal longitudinal variation of both the out-of-plane and the in-plane deflections. These assumptions are appropriate for initial buckling analysis, but reduce the accuracy of subsequent postbuckling analysis. The procedure described in Section 4 identifies the true distributions of the in-plane displacements, strains and stresses, and so enhances the accuracy of each iteration in the VICONOPT postbuckling analysis.

(a)   (b)
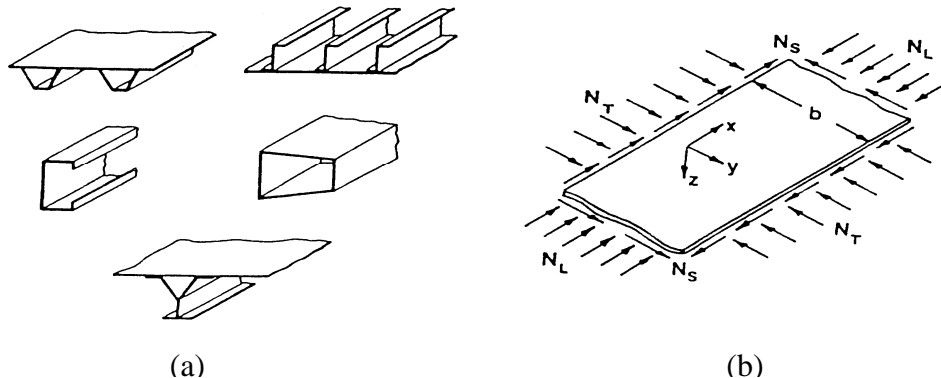
Fig. 1. (a) Prismatic plate assemblies. (b) Component plate, showing in-plane loading.

4 Improved Exact Strip Postbuckling Analysis

Slender aircraft structures such as stiffened panels are often able to carry loads far in excess of their critical buckling loads on account of stress re-distributions across the structure. To minimise the weight of such structures, the postbuckling reserve of strength must therefore be considered. However, due to the assumptions of longitudinal invariance of stress and sinusoidal buckling modes, previous postbuckling analysis with VICONOPT gave good agreement for load and end shortening in initial postbuckling but poor predictions of the associated stress and strain distributions.

In the improvements described here, the governing equilibrium equations are derived and solved analytically for general anisotropic plates, allowing for the effects of bending-membrane coupling. The VIPASA analysis is used, so that the out-of-plane displacements are assumed to vary sinusoidally with a half-wavelength λ, which divides exactly into the plate length a. But, in an extension to Stein's method [2], the in-plane displacements, strains and stress resultants are now assumed to vary as the sums of sinusoidally varying responses with two half-wavelengths λ and $\lambda/2$. By assuming the sinusoidal out-of-plane displacements obtained from the VICONOPT analysis, the in-plane displacements are obtained by solving the in-plane equilibrium equations. Then accurate distributions of the longitudinal, transverse and shear strains and stress resultants are obtained. Finally, energy considerations are used to give equivalent longitudinally invariant stress resultants which will be used in the next iteration of the VICONOPT analysis.

4.1 Description and assumptions of the analysis

At present the postbuckling analysis is restricted to classical plate theory, i.e. no allowance is made for transverse shear deformation. Plates are assumed to have no initial imperfection, but in-plane and out-of-plane anisotropy and curvature effects (i.e. general **A**, **B** and **D** matrices) are permitted. The analysis calculates the variations of the in-plane displacements within the plates; these no longer have the same sinusoidal variation as the out-of-plane displacements, but include contributions with two half-wavelengths and allow for curvature effects in coupled problems. The analysis finds the longitudinal, transverse and shear stress resultants at the longitudinal edges of each strip, i.e. at node level; the strip level values required by VICONOPT are obtained by averaging the values on the two edges of each strip.

4.2 Displacements

Each plate is divided into $n-1$ strips with equal width, and is identified by the n nodes at the strip edges. At each node i, the out-of-plane deflections w_i and rotations ψ_i about the x axis are assumed to vary sinusoidally in the longitudinal direction with half-wavelength λ, and are written in the form

$$\begin{bmatrix} w_i \\ \psi_i \end{bmatrix} = \begin{bmatrix} w_{ic} & w_{is} \\ \psi_{ic} & \psi_{is} \end{bmatrix} \begin{bmatrix} \cos\dfrac{\pi x}{\lambda} \\ \sin\dfrac{\pi x}{\lambda} \end{bmatrix} \tag{5}$$

It is assumed that $\psi_{ij} = w'_{ij}$. The subscript j indicates terms which are to be multiplied by different sinusoidal factors, and prime denotes the derivative with respect to the transverse direction y. The presence of both sine and cosine terms in Eq. (5) allows for the skewing of the nodal lines which occurs for shear-loaded and anisotropic plates. In the absence of shear and anisotropy, w_{ic} and ψ_{ic} are zero.

The in-plane longitudinal (u_i) and transverse (v_i) deflections are assumed to take the form

$$\begin{bmatrix} u_i \\ v_i \end{bmatrix} = \begin{bmatrix} -\bar{\varepsilon}_x \left(x - \dfrac{a}{2} \right) \\ 0 \end{bmatrix} +$$

$$\begin{bmatrix} u_{i0} & u_{ic} & u_{is} & u_{iC} & u_{iS} \\ v_{i0} & v_{ic} & v_{is} & v_{iC} & v_{iS} \end{bmatrix} \begin{bmatrix} 1 \\ \cos\dfrac{\pi x}{\lambda} \\ \sin\dfrac{\pi x}{\lambda} \\ \cos\dfrac{2\pi x}{\lambda} \\ \sin\dfrac{2\pi x}{\lambda} \end{bmatrix} \tag{6}$$

In Eq. (6), the sine and cosine terms with half-wavelength λ occur for coupled laminates with $\mathbf{B}_i \neq 0$, and otherwise can be ignored. The linear term allows for the application of a uniform longitudinal strain $\bar{\varepsilon}_x$.

4.3 Calculation of Strains and Curvatures

The neutral surface strains and curvatures given by von Karman's large deflection theory are

$$
\begin{bmatrix} \varepsilon_{xi} \\ \varepsilon_{yi} \\ \gamma_{xyi} \\ \kappa_{xi} \\ \kappa_{yi} \\ \kappa_{xyi} \end{bmatrix}
=
\begin{bmatrix}
\dfrac{\partial u_i}{\partial x} + \dfrac{1}{2}\left(\dfrac{\partial w_i}{\partial x}\right)^2 \\[2mm]
\dfrac{\partial v_i}{\partial y} + \dfrac{1}{2}\left(\dfrac{\partial w_i}{\partial y}\right)^2 \\[2mm]
\dfrac{\partial u_i}{\partial y} + \dfrac{\partial v_i}{\partial x} + \dfrac{\partial w_i}{\partial x}\dfrac{\partial w_i}{\partial y} \\[2mm]
-\dfrac{\partial^2 w_i}{\partial x^2} \\[2mm]
-\dfrac{\partial^2 w_i}{\partial y^2} \\[2mm]
-2\dfrac{\partial^2 w_i}{\partial x \partial y}
\end{bmatrix}
\tag{7}
$$

$$
=
\begin{bmatrix}
\varepsilon_{xi0} & \varepsilon_{xic} & \varepsilon_{xis} & \varepsilon_{xiC} & \varepsilon_{xiS} \\
\varepsilon_{yi0} & \varepsilon_{yic} & \varepsilon_{yis} & \varepsilon_{yiC} & \varepsilon_{yiS} \\
\gamma_{xyi0} & \gamma_{xyic} & \gamma_{xyis} & \gamma_{xyiC} & \gamma_{xyiS} \\
\kappa_{xi0} & \kappa_{xic} & \kappa_{xis} & \kappa_{xiC} & \kappa_{xiS} \\
\kappa_{yi0} & \kappa_{yic} & \kappa_{yis} & \kappa_{yiC} & \kappa_{yiS} \\
\kappa_{xyi0} & \kappa_{xyic} & \kappa_{xyis} & \kappa_{xyiC} & \kappa_{xyiS}
\end{bmatrix}
\begin{bmatrix}
1 \\ \cos\dfrac{\pi x}{\lambda} \\ \sin\dfrac{\pi x}{\lambda} \\ \cos\dfrac{2\pi x}{\lambda} \\ \sin\dfrac{2\pi x}{\lambda}
\end{bmatrix}
$$

Substituting from Eq. (6) into Eq. (7) gives

$$
\begin{bmatrix} \boldsymbol{\varepsilon}_i \\ \boldsymbol{\kappa}_i \end{bmatrix}
=
\begin{bmatrix} \boldsymbol{\varepsilon}_0(\mathbf{w}_i) \\ \boldsymbol{\kappa}_0(\mathbf{w}_i) \end{bmatrix}
+ \frac{1}{b}\begin{bmatrix} \boldsymbol{\varepsilon}_1 \\ \mathbf{0} \end{bmatrix}\mathbf{u}_i
+ \begin{bmatrix} \boldsymbol{\varepsilon}_2 \\ \mathbf{0} \end{bmatrix}\mathbf{u}_i'
\tag{8}
$$

$$
\mathbf{w}_i = \begin{bmatrix} w_{i0} \\ w_{ic} \\ w_{is} \\ \psi_{i0} \\ \psi_{ic} \\ \psi_{is} \end{bmatrix}, \quad
\mathbf{u}_i = \begin{bmatrix} v_{i0} \\ v_{ic} \\ v_{is} \\ v_{iC} \\ v_{iS} \\ u_{i0} \\ u_{ic} \\ u_{is} \\ u_{iC} \\ u_{iS} \end{bmatrix}
\tag{9,10}
$$

$$
\boldsymbol{\varepsilon}_i = \begin{bmatrix}
\varepsilon_{xi0} \\ \varepsilon_{xic} \\ \varepsilon_{xis} \\ \varepsilon_{xiC} \\ \varepsilon_{xiS} \\
\varepsilon_{yi0} \\ \varepsilon_{yic} \\ \varepsilon_{yis} \\ \varepsilon_{yiC} \\ \varepsilon_{yiS} \\
\gamma_{xyi0} \\ \gamma_{xyic} \\ \gamma_{xyis} \\ \gamma_{xyiC} \\ \gamma_{xyiS}
\end{bmatrix}, \quad
\boldsymbol{\kappa}_i = \begin{bmatrix}
\kappa_{xi0} \\ \kappa_{xic} \\ \kappa_{xis} \\ \kappa_{xiC} \\ \kappa_{xiS} \\
\kappa_{yi0} \\ \kappa_{yic} \\ \kappa_{yis} \\ \kappa_{yiC} \\ \kappa_{yiS} \\
\kappa_{xyi0} \\ \kappa_{xyic} \\ \kappa_{xyis} \\ \kappa_{xyiC} \\ \kappa_{xyiS}
\end{bmatrix}
\tag{11,12}
$$

$$
\boldsymbol{\varepsilon}_0(\mathbf{w}_i) = \begin{bmatrix}
-\bar{\varepsilon}_x + \dfrac{\pi^2}{4\lambda^2}(w_{ic}^2 + w_{is}^2) \\[2mm]
0 \\[1mm]
0 \\[2mm]
\dfrac{\pi^2}{4\lambda^2}(w_{is}^2 - w_{ic}^2) \\[2mm]
-\dfrac{\pi^2}{2\lambda^2} w_{ic} w_{is} \\[2mm]
\dfrac{1}{4}(\psi_{ic}^2 + \psi_{is}^2) \\[2mm]
0 \\[1mm]
0 \\[2mm]
\dfrac{1}{4}(\psi_{ic}^2 - \psi_{is}^2) \\[2mm]
\dfrac{1}{2}\psi_{ic}\psi_{is} \\[2mm]
\dfrac{\pi}{2\lambda}(w_{is}\psi_{ic} - w_{ic}\psi_{is}) \\[2mm]
0 \\[1mm]
0 \\[2mm]
\dfrac{\pi}{2\lambda}(w_{is}\psi_{ic} + w_{ic}\psi_{is}) \\[2mm]
\dfrac{\pi}{2\lambda}(w_{is}\psi_{is} - w_{ic}\psi_{ic})
\end{bmatrix}
\tag{13}
$$

$$\boldsymbol{\kappa}_0(\mathbf{w}_i) = \begin{bmatrix} 0 \\ \dfrac{\pi^2}{\lambda^2} w_{ic} \\ \dfrac{\pi^2}{\lambda^2} w_{is} \\ 0 \\ 0 \\ 0 \\ -\psi'_{ic} \\ -\psi'_{is} \\ 0 \\ 0 \\ 0 \\ -\dfrac{2\pi}{\lambda} \psi_{is} \\ \dfrac{2\pi}{\lambda} \psi_{ic} \\ 0 \\ 0 \end{bmatrix} \tag{14}$$

$$\boldsymbol{\varepsilon}_1 = \begin{bmatrix} \mathbf{J} & \mathbf{O}_5 \\ \mathbf{O}_5 & \mathbf{O}_5 \\ \mathbf{O}_5 & \mathbf{J} \end{bmatrix}, \quad \boldsymbol{\varepsilon}_2 = \begin{bmatrix} \mathbf{O}_5 & \mathbf{O}_5 \\ \mathbf{O}_5 & \mathbf{I}_5 \\ \mathbf{I}_5 & \mathbf{O}_5 \end{bmatrix} \tag{15,16}$$

$$\mathbf{J} = \begin{bmatrix} 0 & 0 & 0 & 0 & 0 \\ 0 & 0 & \omega_i & 0 & 0 \\ 0 & -\omega_i & 0 & 0 & 0 \\ 0 & 0 & 0 & 0 & 2\omega_i \\ 0 & 0 & 0 & -2\omega_i & 0 \end{bmatrix} \tag{17}$$

$$\omega_i = \frac{\pi b_i}{\lambda} \tag{18}$$

where $\mathbf{O}_5$ and $\mathbf{I}_5$ are null and unit matrices of order 5, respectively.

4.4 Stress-Strain Relationships

After obtaining the above expressions for strain and curvature, the stress resultants N_{xi}, N_{yi} and N_{xyi} are needed for the equilibrium equations. For a general anisotropic plate, the in-plane stress-strain relationships at node i take the form

$$\begin{bmatrix} N_{xi} \\ N_{yi} \\ N_{xyi} \end{bmatrix} = \begin{bmatrix} A_{i_{11}} & A_{i_{12}} & A_{i_{16}} \\ A_{i_{12}} & A_{i_{22}} & A_{i_{26}} \\ A_{i_{16}} & A_{i_{26}} & A_{i_{66}} \end{bmatrix} \begin{bmatrix} \varepsilon_{xi} \\ \varepsilon_{yi} \\ \gamma_{xyi} \end{bmatrix} + \begin{bmatrix} B_{i_{11}} & B_{i_{12}} & B_{i_{16}} \\ B_{i_{12}} & B_{i_{22}} & B_{i_{26}} \\ B_{i_{16}} & B_{i_{26}} & B_{i_{66}} \end{bmatrix} \begin{bmatrix} \kappa_{xi} \\ \kappa_{yi} \\ \kappa_{xyi} \end{bmatrix} \tag{19}$$

Substitution from Eq. (8) into Eq. (19) gives

$$\begin{bmatrix} \mathbf{N}_i \\ \mathbf{N}'_i \end{bmatrix} = \bar{\mathbf{A}}_i \begin{bmatrix} \boldsymbol{\varepsilon}_0(\mathbf{w}_i) \\ \boldsymbol{\varepsilon}'_0(\mathbf{w}_i) \end{bmatrix} + \bar{\mathbf{B}}_i \begin{bmatrix} \boldsymbol{\kappa}_0(\mathbf{w}_i) \\ \boldsymbol{\kappa}'_0(\mathbf{w}_i) \end{bmatrix} + \frac{1}{b} \bar{\mathbf{A}}_i \boldsymbol{\varepsilon}_1 \begin{bmatrix} \mathbf{u}_i \\ \mathbf{u}'_i \end{bmatrix} + \bar{\mathbf{A}}_i \boldsymbol{\varepsilon}_2 \begin{bmatrix} \mathbf{u}'_i \\ \mathbf{u}''_i \end{bmatrix} \tag{20}$$

where

$$\mathbf{N}_i = \begin{bmatrix} N_{xi0} \\ N_{xic} \\ N_{xis} \\ N_{xiC} \\ N_{xiS} \\ N_{yi0} \\ N_{yic} \\ N_{yis} \\ N_{yiC} \\ N_{yiS} \\ N_{xyi0} \\ N_{xyic} \\ N_{xyis} \\ N_{xyiC} \\ N_{xyiS} \end{bmatrix} \tag{21}$$

$$\bar{\mathbf{A}}_i = \begin{bmatrix} A_{i_{11}}\mathbf{I}_5 & A_{i_{12}}\mathbf{I}_5 & A_{i_{16}}\mathbf{I}_5 \\ A_{i_{12}}\mathbf{I}_5 & A_{i_{22}}\mathbf{I}_5 & A_{i_{26}}\mathbf{I}_5 \\ A_{i_{16}}\mathbf{I}_5 & A_{i_{26}}\mathbf{I}_5 & A_{i_{66}}\mathbf{I}_5 \end{bmatrix} \tag{22}$$

$$\bar{\mathbf{B}}_i = \begin{bmatrix} B_{i_{11}}\mathbf{I}_5 & B_{i_{12}}\mathbf{I}_5 & B_{i_{16}}\mathbf{I}_5 \\ B_{i_{12}}\mathbf{I}_5 & B_{22}\mathbf{I}_5 & B_{i_{26}}\mathbf{I}_5 \\ B_{i_{16}}\mathbf{I}_5 & B_{i_{26}}\mathbf{I}_5 & B_{i_{66}}\mathbf{I}_5 \end{bmatrix} \tag{23}$$

$\boldsymbol{\varepsilon}_0'(\mathbf{w}_i)$

$$
= \begin{bmatrix}
\dfrac{\pi^2}{2\lambda^2}(w_{ic}\psi_{ic} + w_{is}\psi_{is}) \\[2mm]
0 \\
0 \\[2mm]
\dfrac{\pi^2}{2\lambda^2}(w_{is}\psi_{is} - w_{ic}\psi_{ic}) \\[2mm]
-\dfrac{\pi^2}{2\lambda^2}(w_{is}\psi_{ic} + w_{ic}\psi_{is}) \\[2mm]
\dfrac{1}{2}(\psi_{ic}\psi_{ic}' + \psi_{is}\psi_{is}') \\[2mm]
0 \\
0 \\[2mm]
\dfrac{1}{2}(\psi_{ic}\psi_{ic}' - \psi_{is}\psi_{is}') \\[2mm]
\dfrac{1}{2}(\psi_{is}\psi_{ic}' + \psi_{ic}\psi_{is}') \\[2mm]
\dfrac{\pi}{2\lambda}(w_{is}\psi_{ic}' - w_{ic}\psi_{is}') \\[2mm]
0 \\
0 \\[2mm]
\dfrac{\pi}{2\lambda}(w_{is}\psi_{ic}' + 2\psi_{is}\psi_{ic} + w_{ic}\psi_{is}') \\[2mm]
\dfrac{\pi}{2\lambda}(w_{is}\psi_{is}' + \psi_{is}^2 - w_{ic}\psi_{ic}' - \psi_{ic}^2)
\end{bmatrix}
\qquad (24)
$$

$$
\boldsymbol{\kappa}_0'(\mathbf{w}_i) = \begin{bmatrix}
0 \\[2mm]
\dfrac{\pi^2}{\lambda^2}\psi_{ic} \\[2mm]
\dfrac{\pi^2}{\lambda^2}\psi_{is} \\[2mm]
0 \\
0 \\
0 \\[2mm]
-\psi_{ic}'' \\[2mm]
-\psi_{is}'' \\[2mm]
0 \\
0 \\
0 \\[2mm]
-\dfrac{2\pi}{\lambda}\psi_{is}' \\[2mm]
\dfrac{2\pi}{\lambda}\psi_{ic}' \\[2mm]
0 \\
0
\end{bmatrix}
\qquad (25)
$$

The derivatives $\mathbf{u}_i'$ and $\mathbf{u}_i''$ are obtained by the following finite difference approximations, with

adjustments by parabolic interpolation at the plate edges.

$$
2b_i\mathbf{u}_i' =
\begin{cases}
-3\mathbf{u}_i + 4\mathbf{u}_{i+1} - \mathbf{u}_{i+2} & (i = 1) \\
-\mathbf{u}_{i-1} + \mathbf{u}_{i+1} & (1 < i < n) \\
\mathbf{u}_{i-2} - 4\mathbf{u}_{i-1} + 3\mathbf{u}_i & (i = n)
\end{cases}
\qquad (26)
$$

$$
b_i^2\mathbf{u}_i'' =
\begin{cases}
2\mathbf{u}_i - 5\mathbf{u}_{i+1} + 4\mathbf{u}_{i+2} - \mathbf{u}_{i+3} & (i = 1) \\
\mathbf{u}_{i-1} - 2\mathbf{u}_i + \mathbf{u}_{i+1} & (1 < i < n) \\
\mathbf{u}_{i-3} - 4\mathbf{u}_{i-2} + 5\mathbf{u}_{i-1} - 2\mathbf{u}_i & (i = n)
\end{cases}
\qquad (27)
$$

Explicit expressions for $\mathbf{N}_i$ and $\mathbf{N}_i'$ in terms of $\mathbf{u}_i$ and $\mathbf{w}_i$ are obtained by substituting Eqs. (9)-(16), (22)-(23) and (26)-(27) into Eq. (20).

4.5 Equilibrium Equations

To solve for the in-plane displacements $\mathbf{u}_i$, the in-plane equilibrium conditions for node i are given by

$$
\frac{\partial N_{yi}}{\partial y} + \frac{\partial N_{xyi}}{\partial x} = 0 \qquad (28)
$$

$$
\frac{\partial N_{xyi}}{\partial y} + \frac{\partial N_{xi}}{\partial x} = 0 \qquad (29)
$$

and are expressed in component form by

$$
N_{yi0}' = 0 \qquad (30)
$$

$$
N_{yic}' + \frac{\pi}{\lambda}N_{xyis} = 0 \qquad (31)
$$

$$
N_{yis}' - \frac{\pi}{\lambda}N_{xyic} = 0 \qquad (32)
$$

$$
N_{yiC}' + \frac{2\pi}{\lambda}N_{xyiS} = 0 \qquad (33)
$$

$$
N_{yiS}' - \frac{2\pi}{\lambda}N_{xyiC} = 0 \qquad (34)
$$

$$
N_{xyi0}' = 0 \qquad (35)
$$

$$
N_{xyic}' + \frac{\pi}{\lambda}N_{xis} = 0 \qquad (36)
$$

$$N'_{xyis} - \frac{\pi}{\lambda} N_{xic} = 0 \tag{37}$$

$$N'_{xyiC} + \frac{2\pi}{\lambda} N_{xiS} = 0 \tag{38}$$

$$N'_{xyiS} - \frac{2\pi}{\lambda} N_{xiC} = 0 \tag{39}$$

Substituting the explicit expressions previously obtained for $\mathbf{N}_i$ and $\mathbf{N}'_i$ gives ten equilibrium equations for each node in terms of the in-plane and out-of-plane displacements $\mathbf{u}_i$ and $\mathbf{w}_i$. The equations for each node are assembled into the global equilibrium equations which can be written in matrix form as

$$\mathbf{Hu} = \mathbf{G(w)} \tag{40}$$

where $\mathbf{u}$ includes the unknown in-plane displacements $\mathbf{u}_i$ for all the nodes of the structure, $\mathbf{H}$ is a square matrix with constant coefficients and $\mathbf{G(w)}$ is a non-linear function of the out-of-plane displacements $\mathbf{w}$ which are known from the VICONOPT analysis. Equation (40) is solved to give the in-plane displacements as

$$\mathbf{u} = \mathbf{H}^{-1}\mathbf{G(w)} \tag{41}$$

from which distributions of the in-plane stress resultants $\mathbf{N}_i$ are calculated using Eq. (20).

4.6 Calculation of Equivalent Uniform Stress Resultants

The stress resultants calculated in Section 4.5 cannot be used directly in the next iteration of VICONOPT, because they include sinusoidal terms and so vary in the longitudinal direction. So equivalent longitudinally invariant stress resultants are calculated as follows, based on energy considerations.

The work done by the applied loading at node i is given by

$$V = V_{xi} + V_{yi} + V_{xyi} \tag{42}$$

where

$$V_{xi} = b_i \int_0^\lambda N_{xi}\varepsilon_{xi}\,dx \tag{43}$$

$$V_{yi} = b_i \int_0^\lambda N_{yi}\varepsilon_{yi}\,dx \tag{44}$$

$$V_{xyi} = b_i \int_0^\lambda N_{xyi}\gamma_{xyi}\,dx \tag{45}$$

Writing the stress resultants as

$$\begin{bmatrix} N_{xi} \\ N_{yi} \\ N_{xyi} \end{bmatrix} = \begin{bmatrix} N_{xi0} & N_{xic} & N_{xis} & N_{xiC} & N_{xiS} \\ N_{yi0} & N_{yic} & N_{yis} & N_{yiC} & N_{yiS} \\ N_{xyi0} & N_{xyic} & N_{xyis} & N_{xyiC} & N_{xyiS} \end{bmatrix} \begin{bmatrix} 1 \\ \cos\dfrac{\pi x}{\lambda} \\ \sin\dfrac{\pi x}{\lambda} \\ \cos\dfrac{2\pi x}{\lambda} \\ \sin\dfrac{2\pi x}{\lambda} \end{bmatrix} \tag{46}$$

and substituting Eqs. (8)-(16) and (46) into Eqs. (43)-(45), the components of V are written as

$$V_{xi} = N_{xi0}\eta_{xi0} + N_{xic}\eta_{xic} + N_{xis}\eta_{xis} + N_{xiC}\eta_{xiC} + N_{xiS}\eta_{xiS} \tag{47}$$

$$V_{yi} = N_{yi0}\eta_{yi0} + N_{yic}\eta_{yic} + N_{yis}\eta_{yis} + N_{yiC}\eta_{yiC} + N_{yiS}\eta_{yiS} \tag{48}$$

$$V_{xi} = N_{xyi0}\eta_{xyi0} + N_{xyic}\eta_{xyic} + N_{xyis}\eta_{xyis} + N_{xyiC}\eta_{xyiC} + N_{xyiS}\eta_{xyiS} \tag{49}$$

where the parameters η_{xij}, η_{yij} and η_{xyij}, listed in Appendix A, are expressed in terms of the known quantities $\bar{\varepsilon}_x$, $\mathbf{u}_i$ and $\mathbf{w}_i$.

Comparing with the corresponding expressions for uniform loading yields the following expressions for equivalent longitudinally invariant stress resultants, which are used by VICONOPT to calculate the strip stiffness matrices.

$$\bar{N}_{xi} = N_{xi0} + \frac{1}{\eta_{xi0}}\begin{pmatrix} N_{xic}\eta_{xic} + N_{xis}\eta_{xis} \\ +N_{xiC}\eta_{xiC} + N_{xiS}\eta_{xiS} \end{pmatrix} \tag{50}$$

$$\bar{N}_{yi} = N_{yi0} +$$
$$\frac{1}{\eta_{yi0}} \begin{pmatrix} N_{yic}\eta_{yic} + N_{yis}\eta_{yis} \\ +N_{yic}\eta_{yic} + N_{yiS}\eta_{yiS} \end{pmatrix} \quad (51)$$

$$\bar{N}_{xyi} = N_{xyi0} +$$
$$\frac{1}{\eta_{xyi0}} \begin{pmatrix} N_{xyic}\eta_{xyic} + N_{xyis}\eta_{xyis} \\ +N_{xyic}\eta_{xyic} + N_{xyiS}\eta_{xyiS} \end{pmatrix} \quad (52)$$

4.7 Calculation of Stress Resultant Derivatives

The Newton iterations of VICONOPT require derivatives of the global stiffness matrix **K** with respect to the out-of-plane displacements. These derivatives are calculated by a finite difference procedure in which the out-of-plane displacement components w_k (representing w_{ic}, w_{is}, ψ_{ic} and ψ_{is} for each node i) are perturbed in turn, resulting in perturbations of the effective stress resultants derived in Eqs. (50)-(52). In order to calculate these perturbations, it is not necessary to repeat the whole analysis of Section 4; instead they can be calculated analytically by obtaining the derivatives of $\mathbf{N}_i$ with respect to each component w_k.

   Differentiating Eq. (20) gives

$$\frac{\partial \mathbf{N}_i}{\partial w_k} = \bar{\mathbf{A}}_i \frac{\partial \boldsymbol{\varepsilon}_0(\mathbf{w}_i)}{\partial w_k} + \bar{\mathbf{B}}_i \frac{\partial \boldsymbol{\kappa}_0(\mathbf{w}_i)}{\partial w_k}$$
$$+ \frac{1}{b} \bar{\mathbf{A}}_i \boldsymbol{\varepsilon}_1 \frac{\partial \mathbf{u}_i}{\partial w_k} + \bar{\mathbf{A}}_i \boldsymbol{\varepsilon}_2 \frac{\partial \mathbf{u}'_i}{\partial w_k} \quad (53)$$

in which the first two terms on the right-hand side can be obtained by differentiating Eqs. (13) and (14), respectively with respect to w_k. The third term is obtained by differentiating Eq. (41) to give

$$\frac{\partial \mathbf{u}}{\partial w_k} = \mathbf{H}^{-1} \frac{\partial \mathbf{G}(\mathbf{w})}{\partial w_k} \quad (54)$$

noting that the previously inverted matrix can be re-used for these calculations. Finally, the fourth term of Eq. (53) is obtained from the third term by the use of finite difference approximations analogous to those of Eq. (26).

5 Illustrative Results

This section gives illustrative results for an isotropic square plate loaded in longitudinal compression. All four edges were simply supported with respect to out-of-plane displacement. The plate had length and width $0.3\,\mathrm{m}$, thickness $0.001\,\mathrm{m}$, Young's modulus $110\,\mathrm{kNmm^{-2}}$ and Poisson's ratio 0.3. For postbuckling analysis the plate was divided into 10 longitudinal strips of equal width.

N_x

N_y

Fig. 2. Variation of stress resultants across the neutral surface of a square isotropic plate postbuckling in longitudinal compression, with all edges simply supported against out-of-plane deflection and the longitudinal edges fixed in-plane.

N_x : present analysis

N_y : present analysis

N_x : previous VICONOPT analysis [9]

N_y : previous VICONOPT analysis [9]

N_x : finite element analysis [11]

N_y : finite element analysis [11]
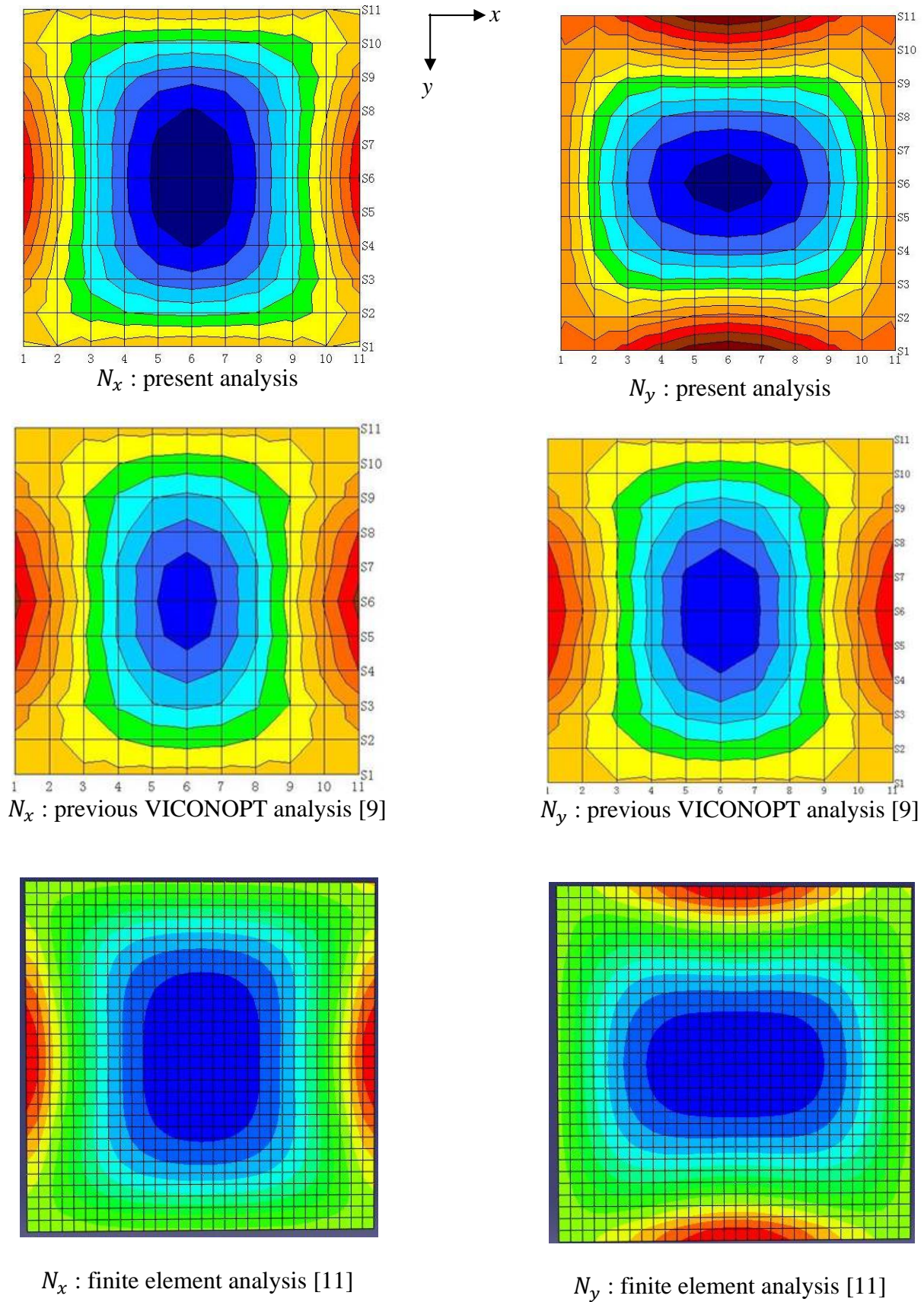
Fig. 3. Variation of stress resultants across the top surface of a square isotropic plate postbuckling in longitudinal compression, with all edges simply supported against out-of-plane deflection and the longitudinal edges fixed in-plane.

N_x : present analysis

N_y : present analysis

N_x : previous VICONOPT analysis [9]

N_y : previous VICONOPT analysis [9]

N_x : finite element analysis [11]

N_y : finite element analysis [11]
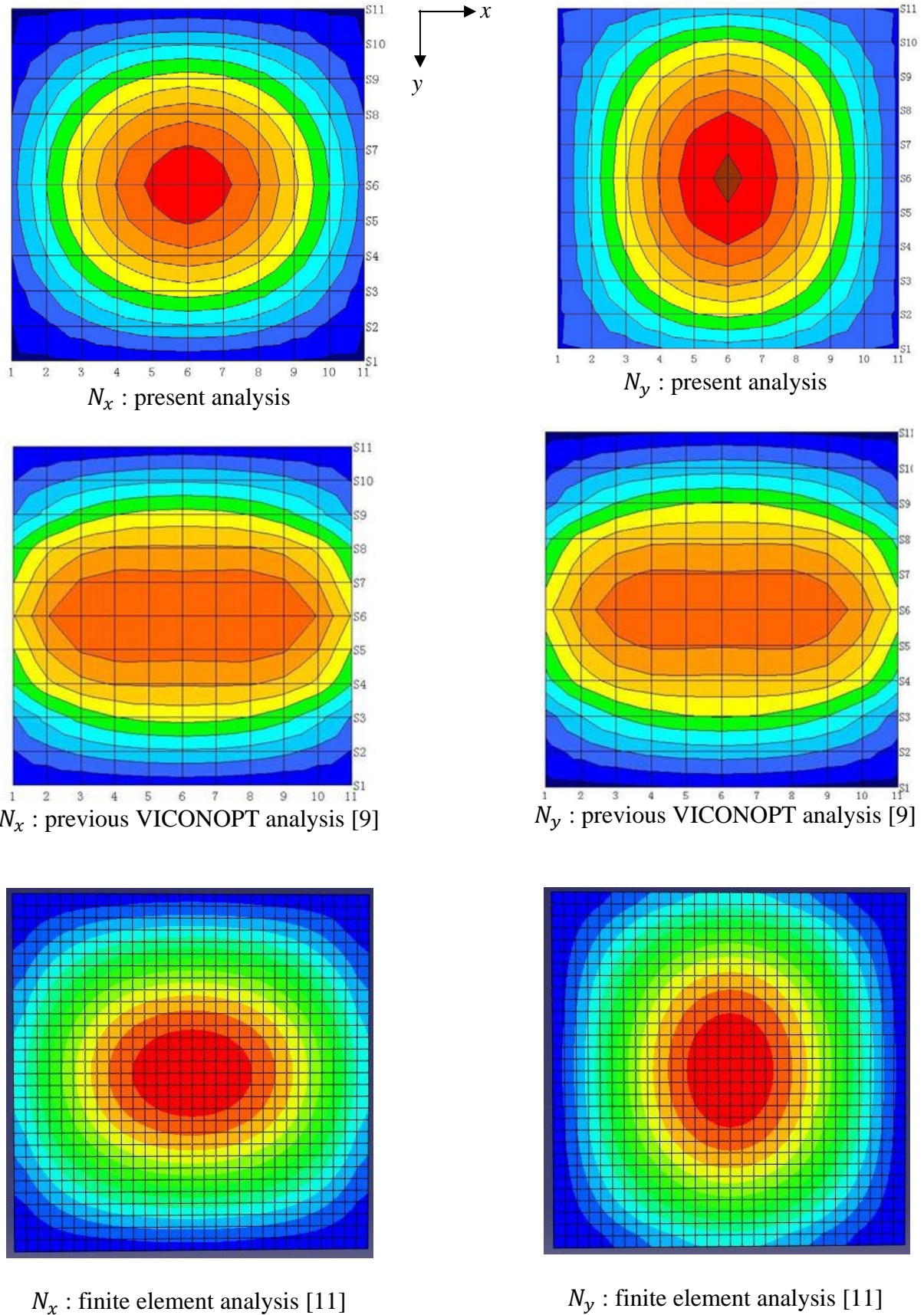
Fig. 4. Variation of stress resultants across the bottom surface of a square isotropic plate postbuckling in longitudinal compression, with all edges simply supported against out-of-plane deflection and the longitudinal edges fixed in-plane.

11

In order to simulate the intended use of the improved analysis, a postbuckling analysis was carried out using the previous version of VICONOPT [9]. At cycle 10, when the longitudinal strain exceeded the initial buckling strain by 45.1%, the out-of-plane displacements **w** were saved and used as input to the procedure described in Section 4. The distributions of the N_x and N_y stress resultants were found, together with the effective longitudinally invariant distributions to be used in the next iteration of the VICONOPT postbuckling analysis. In the figures below these distributions are shown graphically to give a qualitative indication of the postbuckling behaviour of the plate. In the contour plots, blue shading denotes increasing compression while red indicates decreasing compression (which usually results in regions of tension on the bottom surface).

5.1   Longitudinal Edges Fixed In-Plane

In the first example, the longitudinal edges of the plate are fixed in-plane, i.e. in the solution of Eq. (40) all components of $\mathbf{u}_i$ are forced to zero at nodes $i = 1$ and $i = n$. The resulting distributions of N_x and N_y are shown in Fig. 2, where it is seen that N_x is almost longitudinally invariant but N_y is not.

It should be noted that all the strains and stress resultants calculated in Section 4 are those at the neutral surface. In practice the stresses vary through the thickness on account of the curvature, taking their greatest values at the surfaces of the plate. Figures 3 and 4 show the variation of N_x and N_y at the top and bottom surfaces, respectively, and additionally validate the method by comparison with previous VICONOPT results [9] and FE results obtained with the software ABAQUS [11]. It is seen that the present method gives much closer agreement to the FE results than does the previous VICONOPT analysis.

5.2   Other In-Plane Edge Conditions

The plate was analysed for two further in-plane edge conditions. In both cases longitudinal displacement was prevented at the longitudinal edges, i.e. $u_i = 0$ for nodes $i = 1$ and $i = n$. In the first case there was no restraint against transverse displacement. In the second case the longitudinal edges were held straight, so that v_{i0} could be non-zero at these nodes but the other components of v_i were zero. Top and bottom surface distributions of N_x and N_y are shown for these two cases in Figs. 5 and 6, respectively. Again it can be seen that there is a considerable variation of the stress resultants in both directions, which should be taken into account when following the postbuckling path. This has been done while calculating the effective uniform stress resultants of Section 4.6, which are therefore expected to provide accurate estimates of the postbuckling stiffness of the plate.

6   Concluding Remarks

Exact strip analysis provides an efficient approach to postbuckling analysis of isotropic and anisotropic plate assemblies for use in the preliminary design of aircraft structures. This paper has presented a theoretical improvement to exact strip postbuckling analysis, which enhances the accuracy of mode shapes, strain and stress distributions. Illustrative numerical results have been presented for an isotropic plate with various edge conditions and show good agreement with finite element results. The method will be further assessed by considering fully anisotropic plates with combined loading conditions.

The purpose of the work is to provide an enhanced procedure for calculating effective longitudinally invariant stresses and their derivatives for use in the exact strip software VICONOPT. Implementation of the method into the VICONOPT code is currently in progress. When this task is completed, the method will be fully assessed by using it in a complete postbuckling analysis. It will then be further extended to the analysis of stiffened panels, to provide additional capabilities for aircraft designers.
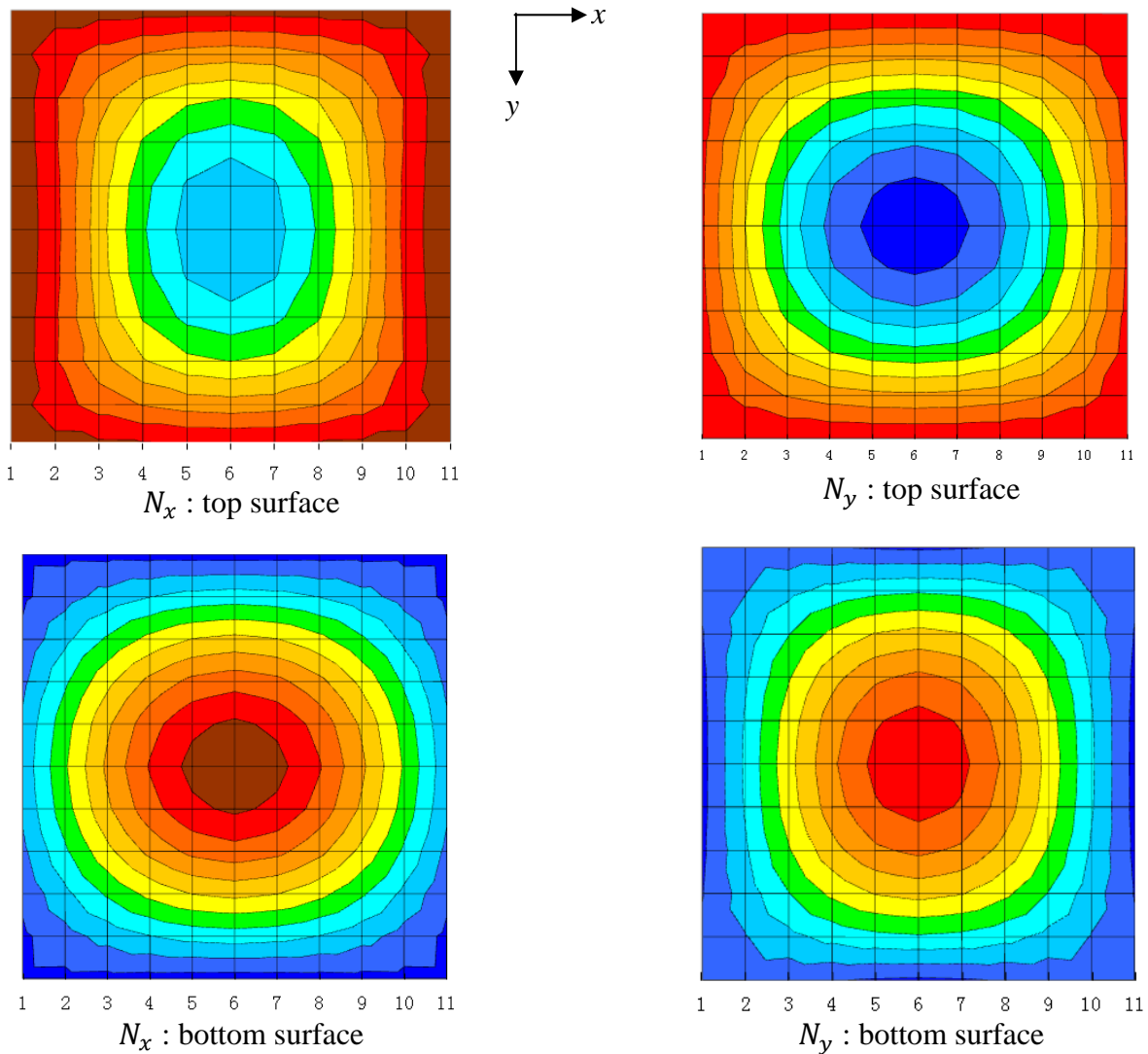
Fig. 5. Variation of stress resultants across the top and bottom surfaces of a square isotropic plate postbuckling in longitudinal compression, with all edges simply supported against out-of-plane deflection and the longitudinal edges free.

References

[1] Williams FW and Wittrick WH. An algorithm for computing critical buckling loads of elastic structures. *Journal of Structural Mechanics*, Vol. 1. No. 4, pp 497-519, 1973.

[2] Stein M. Analytical results for post-buckling behaviour of plates in compression and in shear. In: *Aspects of the analysis of plate structures, A volume in honour of W. H. Wittrick* (ed. DJ Dawe, RW Horsington, AG Kamtekar and GH Little), Clarendon Press, Oxford, 1985, pp 205-223.

[3] Kennedy D, Fischer M and Featherston CA. Recent developments in exact strip analysis and optimum design of aerospace structures. *Proceedings of IMechE Part C: Journal of Mechanical Engineering Science,* Vol. 221, No. 4, pp 399-413, 2007.

[4] Wittrick WH and Williams FW. Buckling and vibration of anisotropic or isotropic plate assemblies under combined loadings. *International Journal of Mechanical Sciences*, Vol. 19, No. 4, pp 209-223, 1974.

[5] Anderson MS and Kennedy D. Transverse shear deformation in exact buckling and vibration of composite plate assemblies. *AIAA Journal*, Vol. 31, No. 10, pp 1963-1965, 1993.

[6] Williams FW and Kennedy D. Reliable use of determinants to solve non-linear structural eigenvalue problems efficiently. *International Journal for Numerical Methods in Engineering*, Vol. 26, No. 8, pp 1825-1841, 1988.
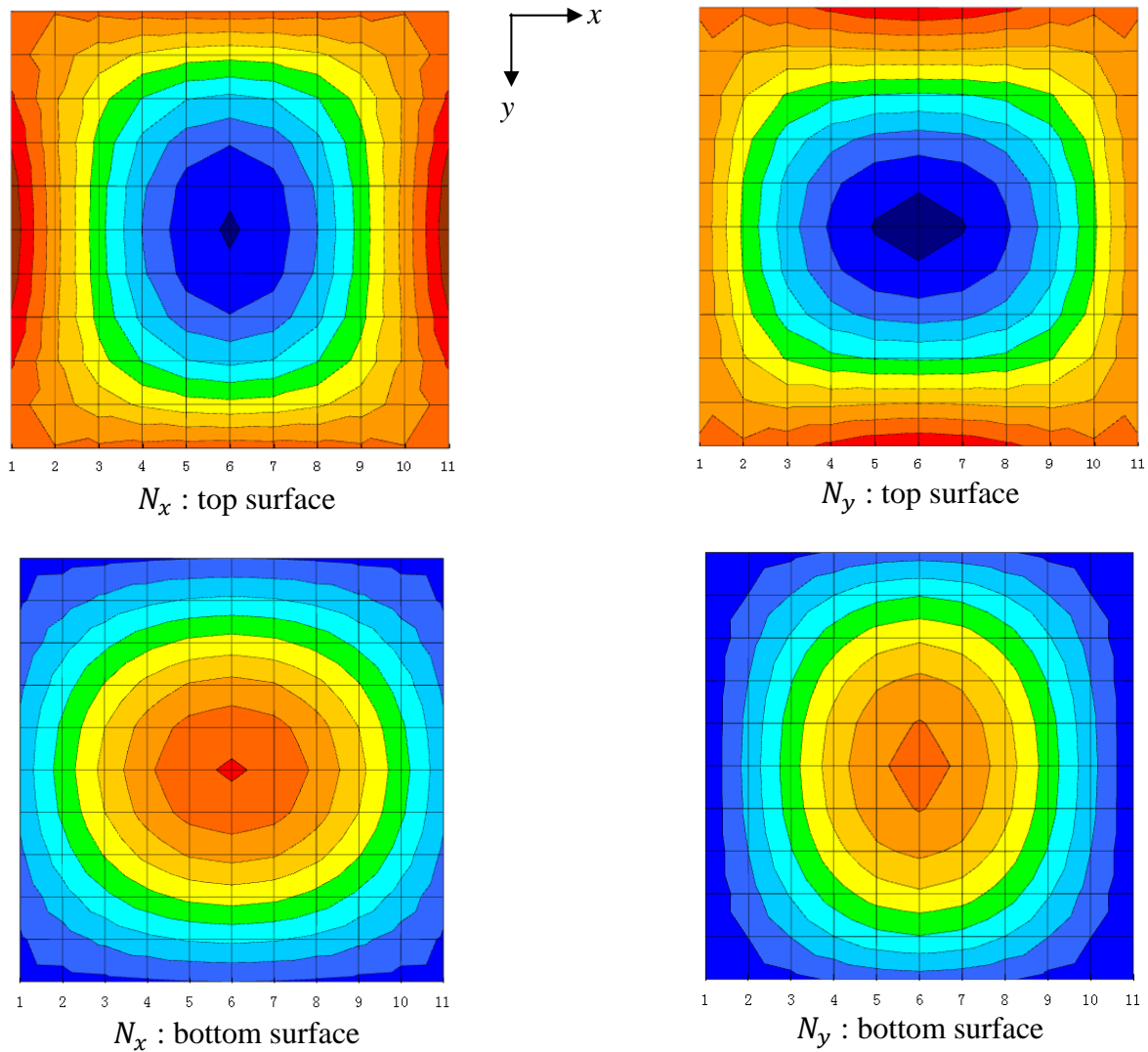
Fig. 6. Variation of stress resultants across the top and bottom surfaces of a square isotropic plate postbuckling in longitudinal compression, with all edges simply supported against out-of-plane deflection and the longitudinal edges held straight.

[7] Anderson MS, Williams FW and Wright CJ. Buckling and vibration of any prismatic assembly of shear and compression loaded anisotropic plates with an arbitrary supporting structure. *International Journal of Mechanical Sciences,* Vol. 25, No. 8, pp 585-596, 1983.

[8] Powell SM, Williams FW, Askar A-S and Kennedy D. Local postbuckling analysis for perfect and imperfect longitudinally compressed plates and panels. *Proceedings of 39th AIAA/ASME/ASCE/AHS/ASC Structures, Structural Dynamics, and Materials Conference*, Long Beach, pp 595-603, 1998.

[9] Anderson MS and Kennedy D. Postbuckling of composite stiffened panels using exact strip analysis with Newton iteration. *Proceedings of 49th AIAA/ASME/ASCE/AHS/ASC Structures, Structural Dynamics, and Materials Conference*, Schaumburg, Paper AIAA-2008-2194, pp. 1-8, 2008.

[10] Qu S, Kennedy D and Featherston CA. Multilevel optimisation of an aircraft wing incorporating postbuckling effects. *Proceedings of CEAS European Air and Space Conference*, Manchester, UK, pp 1-10, 2009.

[11] *ABAQUS/Standard User's Manual, Version 6.8.* Hibbitt, Karlsson and Sorensen, Inc., Pawtucket, 2008.

Appendix A

Coefficients in equivalent uniform stress resultants calculations

$$\eta_{xi0} = -\lambda \bar{\varepsilon}_x - 2u_{ic} + \frac{\pi^2}{4\lambda}(w_{ic}^2 + w_{is}^2) \tag{A1}$$

$$\eta_{xic} = \frac{\pi}{2} u_{is} - \frac{8}{3} u_{iC} - \frac{2\pi}{3\lambda} w_{ic} w_{is} \tag{A2}$$

$$\eta_{xis} = -\frac{2\lambda}{\pi} \bar{\varepsilon}_x - \frac{\pi}{2} u_{ic} - \frac{4}{3} u_{iS} \\ + \frac{\pi}{3\lambda}(w_{ic}^2 + w_{is}^2) \tag{A3}$$

$$\eta_{xiC} = \frac{2}{3} u_{ic} + \pi u_{iS} + \frac{\pi^2}{8\lambda}(w_{is}^2 - w_{ic}^2) \tag{A4}$$

$$\eta_{xiS} = \frac{4}{3} u_{is} - \pi u_{iC} - \frac{\pi^2}{4\lambda} w_{ic} w_{is} \tag{A5}$$

$$\eta_{yi0} = \lambda v_{i0}' + \frac{2\lambda}{\pi} v_{is}' + \frac{\lambda}{4}(\psi_{ic}^2 + \psi_{is}^2) \tag{A6}$$

$$\eta_{yic} = \frac{\lambda}{2} v_{i0}' + \frac{4\lambda}{3\pi} v_{is}' + \frac{2\lambda}{3\pi} \psi_{ic} \psi_{is} \tag{A7}$$

$$\eta_{yis} = \frac{2\lambda}{\pi} v_{i0}' + \frac{\lambda}{2} v_{is}' - \frac{2\lambda}{3\pi} v_{iC}' \\ + \frac{\lambda}{3\pi}(\psi_{ic}^2 + 2\psi_{is}^2) \tag{A8}$$

$$\eta_{yiC} - \frac{2\lambda}{3\pi} v_{is}' + \frac{\lambda}{2} v_{iC}' + \frac{\lambda}{8}(\psi_{ic}^2 - \psi_{is}^2) \tag{A9}$$

$$\eta_{yiS} = \frac{4\lambda}{3\pi} v_{ic}' + \frac{\lambda}{2} v_{is}' + \frac{\lambda}{4} \psi_{ic} \psi_{is} \tag{A10}$$

$$\eta_{xyi0} = \lambda u_{i0}' + \frac{2\lambda}{\pi} u_{is}' - 2v_{ic} \\ + \frac{\pi}{2}(w_{is} \psi_{ic} - w_{ic} \psi_{is}) \tag{A11}$$

$$\eta_{xyic} = \frac{\lambda}{2} u_{ic}' + \frac{4\lambda}{3\pi} u_{is}' + \frac{\pi}{2} v_{is} - \frac{8}{3} v_{iC} \\ + \frac{2}{3}(w_{is} \psi_{is} - w_{ic} \psi_{ic}) \tag{A12}$$

$$\eta_{xyis} = \frac{2\lambda}{\pi} u_{i0}' + \frac{\lambda}{2} u_{is}' - \frac{2\lambda}{3\pi} u_{ic}' - \frac{\pi}{2} v_{ic} \\ - \frac{4}{3} v_{is} - \frac{1}{3}(w_{is} \psi_{ic} + 7w_{ic} \psi_{is}) \tag{A13}$$

$$\eta_{xyiC} = -\frac{2\lambda}{3\pi} u_{is}' + \frac{\lambda}{2} u_{ic}' + \frac{2}{3} v_{ic} \\ + \frac{\pi}{4} v_{is} + \pi(w_{is} \psi_{ic} + w_{ic} \psi_{is}) \tag{A14}$$

$$\eta_{xyiS} = \frac{4\lambda}{3\pi} u_{ic}' + \frac{\lambda}{2} u_{is}' + \frac{4}{3} v_{is} - \pi v_{iC} \\ + \frac{\pi}{4}(w_{is} \psi_{is} - w_{ic} \psi_{ic}) \tag{A15}$$

Copyright Statement